Int. J. Electrochem. Sci., 11 **(2016)** 4050 - 4075

International Journal of
ELECTROCHEMICAL
SCIENCE
www.electrochemsci.org

Synthesis and Evaluation of New Isoxazolidine Derivatives of Aldehyde as Corrosion Inhibitors for Mild Steel Corrosion in Acidic and Saline Media

Mohammad A. Jafar Mazumder

Chemistry Department, King Fahd University of Petroleum & Minerals, Dhahran 31261, Saudi Arabia
E-mail: jafar@kfupm.edu.sa

Received: 2 December 2015 / *Accepted:* 11 February 2016 / *Published:* 1 April 2016

A new series of isoxazolidine derivatives of aldehyde were synthesized using a nitrone cycloaddition reaction. The corrosion inhibition efficiency of these synthesized compounds on mild steel were determined using a gravimetric method, linear polarization resistance, Tafel extrapolation method, electrochemical impedance spectroscopy, and surface tension in various solutions of the inhibitors in 1 M HCl, 0.5 M H_2SO_4, and CO_2-saturated 0.5 M NaCl (40 °C, 1 atm; 120 °C, 9.9 atm). The *p*-9-[hexahydropyrrolo(1,2-b)isoxazol-2-yl]nonyloxybenzaldehyde performed the best in comparison to the other synthesized inhibitors and two commercial inhibitors. The anodic shift of the E_{corr} values, and the larger reduction of i_{corr} values in the anodic side of the Tafel plots, suggest that the inhibitor molecules acted primarily as anodic inhibitors. The ΔG^{o}_{ads} points towards both physisorption as well as chemisorption of the inhibitors on the metal surface. The inhibitor molecules are best fitted by a Temkin adsorption isotherm in both acids, while the Langmuir adsorption isotherm performed best in a CO_2-saturated saline media. The surface tension confirms that the inhibitor molecules form a film at the metal's surface. The surface coverage data and CMC values demonstrate that the inhibitor molecules undergo adsorption on the metal surface, rather than micellization.

Keywords: Corrosion inhibitors; Potentiodynamic polarization; Electrochemical impedance; Acidic medium; Saline medium.

1. INTRODUCTION

Corrosion is a process that damages metal due to a chemical reaction with the environment [1-3]. It is a constant, continuous and costly problem [4], often difficult to eliminate completely. Crude oil is corrosive towards iron and mild steel, which are widely used in the petroleum industry. Approximately 25 to 30% of the total economic losses in the oil and gas industry are due to failure of

doi: 10.20964/110257

pipes and other plant systems resulting from metallic corrosion [5,6]. In addition, corrosion can lead to serious accidents, explosions and environmental damage. Concerns with the corrosion of mild steel and iron receive particular attention in the academic and industrial community due to their remarkable industrial applications. Acid solutions are used in the refining of crude oil, which usually attack the equipment surface. The other important industrial applications of acid are oil-well acid in oil recovery, industrial acid cleaning, acid pickling, acid descaling and etching of metal alloys [7,8]. It is obvious that an environment containing acid, gases (H_2S, CO_2), moisture and dissolved salts, when operated at high temperature, has a potential of corroding metal pipelines. To protect metals from corrosion, a number of methods are being used; namely, cathodic protection, anodic protection, galvanization, organic and inorganic coatings, ceramic/glass linings and the addition of inhibitors. Corrosion inhibitors are often used to prevent or minimize both metal dissolution and acid consumption to protect oil and gas pipelines [9,10]. Currently, there is a plethora of corrosion inhibitors to alleviate the problem; however, room exists for new products that are cheaper, environmentally friendly and offer increased corrosion protection.

The selection of effective corrosion inhibitors and their efficient applications is one of the most important and economic methods to minimize metallic corrosion in a hostile environment [11,12]. Environmental issues have led to an increase in the use of organic inhibitors as replacements for the highly toxic inorganic inhibitors, such as chromium compounds. Protection from corrosive attacks on metallic materials has been successfully achieved by the use of oxygen, sulfur and nitrogen-containing organic compounds, which are commonly used in industrial acid cleaning, oil-well acid in oil recovery, acid descaling, acid pickling, and etching of metal alloys [13,14]. The organic inhibitors may undergo physi- or chemisorption on the metal surface, by displacing water molecules on the surface to form a compact barrier film [15], or by the formation of a coordinate covalent bond via the interaction of the nonbonded (lone pair) and π-electrons in the inhibitor molecules with the vacant d-orbitals of the metal [16].

The significant inhibitory effect of corrosion inhibitors is strengthened by the presence of two functionalities – heteroatoms (N, O, P, or S) of high electron density and hydrophobes of long alkyl chains [17-19]. The strength of adsorption of these molecules onto the surface of the metals depends on structural features of heteroatoms, which include the planarity (p) and lone pairs of electrons present on N, O and S atoms [20]. Some researchers suggest that the length of the hydrophobic alkyl chain plays a great role, while others indicate the opposite [21,22]. Recent studies have shown that the corrosion protection ability of the organic compounds containing polar functional groups is enhanced in the presence of heterocyclic compounds having polar groups and π-electrons [23].

To the best of our knowledge, a limited number of organic inhibitors showed a similar efficacy in preventing corrosive attacks on mild steel in hydrochloric acid (HCl), as well as in sulfuric acid (H_2SO_4) media [24,25]. Typically, the inhibitors perform well in HCl but behave poorly in H_2SO_4, and vice versa [26]. The present mechanistic understanding and practical implications of CO_2 corrosion of carbon and low-alloy steels is complex. The poorly understood complex mechanism of CO_2 corrosion appears to make the designing of new inhibitors more difficult [27,28]. In recent years, the organic compounds containing isoxazolidine have received huge interest for the potential application in oil and gas industry. A variety of isoxazolidines [29-32] have been synthesized and tested for the inhibition

action on the corrosion of mild steel in 1 M HCl, using weight loss and polarization techniques. The number of organic compounds containing isoxazolidine [33-36] and diallylammonium moieties [37] have been reported for corrosion inhibition of mild steel in 1 M HCl and/or 0.5 M H_2SO_4 media. Recently we investigated isoxazolidine containing a cationic charge, hydrophobe, alkyne functionality and cinnamyl motifs in a single molecular framework, and evaluated their effectiveness in arresting corrosive attacks on mild steel in both acidic and CO_2-saturated saline media [38].

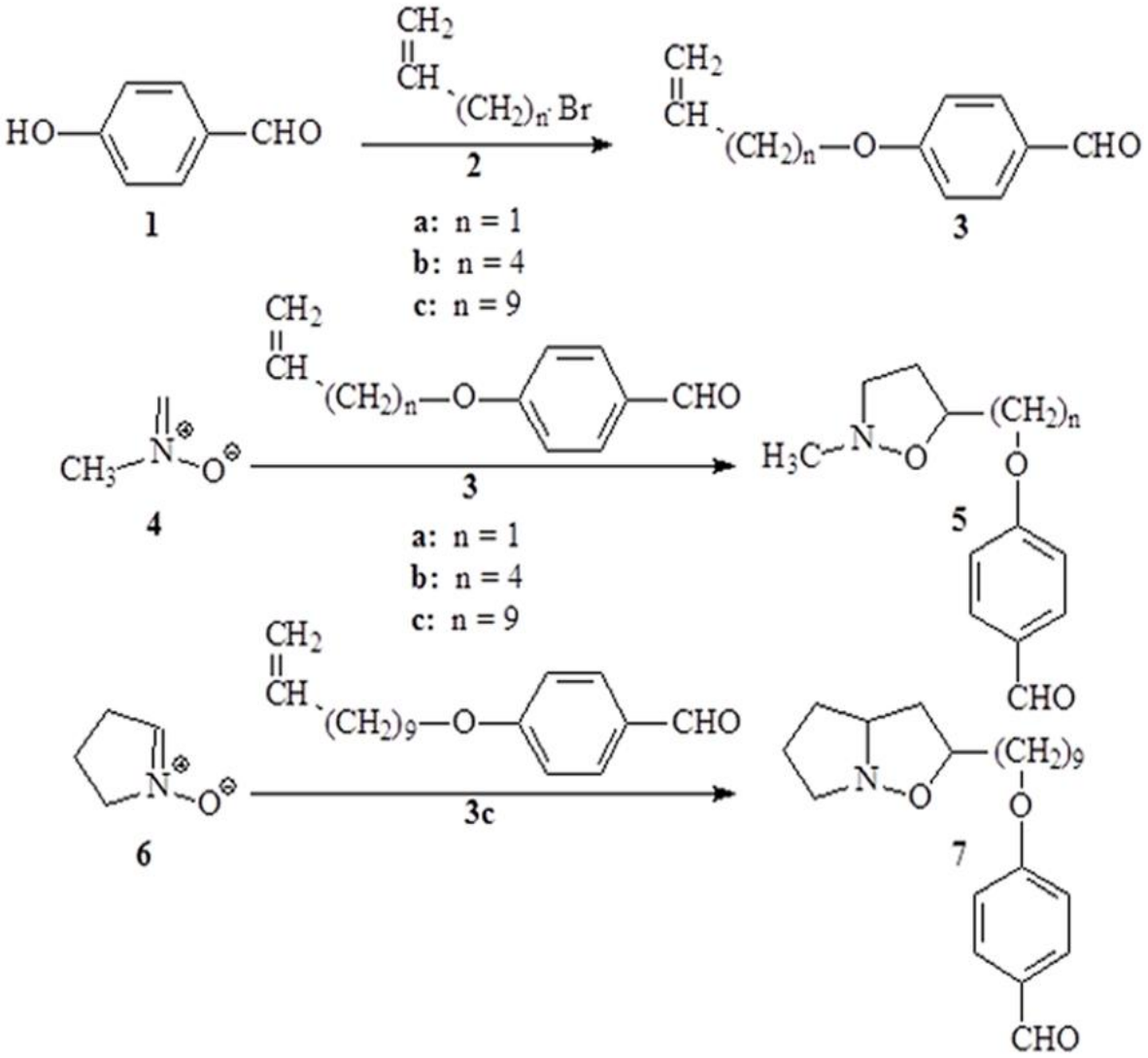

Figure 1. Synthesis of inhibitor molecules.

Herein, the aim of this study is to synthesize a special class of isoxazolidines from inexpensive and commercially available starting materials: *p*-hydroxybenzaldehyde, flexible chain lengths of bromoalkenes $Br(CH_2)_nCH=CH_2$ (n = 1, 4, 9) and precursor of different nitrones, as outlined in Fig. 1, with the intention that they be used as corrosion inhibitors in both acidic and in saline media. The molecular design of these new isoxazolidines, containing multiple donor atoms (N, O), π-electrons, aldehyde functionality, and adjustable chain lengths of hydrophobes, with an alkyl group or aliphatic

bicyclic structure having high surface area, were used to study their efficiency on the corrosion inhibition of iron in acidic (e. g.; HCl, H_2SO_4) media and carbonated brine solution. Corrosion inhibition efficiencies were determined by gravimetric weight loss, potentiodynamic polarizations, electrochemical impedance spectroscopy and surface tension. These methods allowed us to examine the effects of differing chain lengths of hydrophobes, with an alkyl group or aliphatic bicyclic structure in the compounds, on the inhibition in acidic and/or CO_2-saturated sodium chloride solutions. We anticipated that the outcome of this study would lead to better corrosion inhibitors that would have a potential utilization in the oil and gas industries.

2. EXPERIMENTAL

2.1. Materials

N-methylhydroxylamine hydrochloride, paraformaldehyde, pyrrolidine, allyl bromide, 6-bromo-1-hexene, 11-bromo-1-undecene, *p*-hydroxybenzaldehyde obtained from Fluka Chemie AG, were used as received. Sodium metal, mercury (II) oxide and selenium dioxide obtained from Aldrich chemical, sodium acetate trihydrate, sodium bicarbonate ($NaHCO_3$), sodium sulfate (Na_2SO_4) and sodium chloride (NaCl) obtained from Fluka Chemie AG, were used as received. *N*-hydroxypyrrolidine obtained from BDH Chemical Ltd (Pool, England), was used as received. Ethanol, methanol, ether and toluene were purchased from Sigma Aldrich chemicals, and were used as received. All solvents were of HPLC grade. Sodium hydroxide (NaOH), hydrochloric acid (HCl) and sulfuric acid (H_2SO_4) solutions were purchased as concentrates from Fisher Scientific Company, and were used as received. Silica gel 100 was purchased from Fluka Chemie AG. Water was purified and de-ionized using a Milli-Q system from Millipore. All glassware was cleaned using de-ionized water.

2.2. Physical Methods

Digital Melting Point Apparatus (Electro thermal- IA9100) recorded the melting points using heating rates of 1 °C min^{-1} in the vicinity of the melting points. The structural composition was determined by FT-IR (Perkin Elmer 16F PC FTIR), and the chemical composition was determined by a ^{1}H and ^{13}C NMR (JEOL LA 500 MHz) spectrometer. A Perkin Elmer Elemental Analyzer (Carlo-Erba: Model 2400) was used to analyze the elemental composition. A computer-controlled potentiostat-galvanostat (Auto Lab, Booster 10A-BST707A, Eco Chemie, Netherlands) was used for the electrochemical measurements. A R&D Autoclave Bolted Closure System (Model # 401C-0679, Autoclave Engineers) equipped with PC and monitor, and FID control system fitted with a microcomputer (High Tech Engineering, India) was used to study the corrosion inhibition efficiencies under high temperature and pressure. A surface tensiometer (PHYWE, Germany) was used to measure the surface tension. All the reactions were carried out under a positive atmosphere of N_2.

2.3. Synthesis

2.3.1. General procedure for the preparation of p-allyloxybenzaldehydes (3a)

Sodium ethoxide (0.13 mol) was prepared by the addition of sodium (3.0 g) in ethanol (65 ml), which was then added to *p*-hydroxybenzaldehyde (1) (15.9g, 0.13 mol) while stirring at room temperature, to form a homogeneous mixture. The allyl bromide (2a) (15.7g, 0.13 mol) was added to the homogeneous mixture, the temperature was raised to 65 °C and heat was applied to the reaction mixture for 12 h. After the time elapsed, most of the ethanol was removed by a gentle steaming of N_2. The residual reaction mixture was dissolved in ether (50 ml), and then washed with de-ionized water (2×100 ml), followed by 1.5 M NaOH solution (2x50 ml), and de-ionized water (2×50 ml), respectively. The organic layer was dried (Na_2SO_4) and concentrated to give *p*-allyloxybenzaldehyde (3a) as a brown liquid. ^{1}H NMR spectrum has shown that the product (3a) is very pure, and used without further purification; the yield was 18.7 g (88.7%). (Found: C, 74.0; H, 6.1. $C_{10}H_{10}O_2$ requires C, 74.06; H, 6.21%). $\nu_{max.}$ (neat) 3075, 2828, 2738, 1688, 1600, 1576, 1507, 1459, 1425, 1393, 1365, 1313, 1259, 1160, 1112, 995, 933, 856, 834, 762, and 656 cm^{-1}. δ_H ($CDCl_3$): 4.62 (2H, d, J 5.2 Hz), 5.34 (2H, m), 6.06 (1H, m), 7.03 (2H, d, J 8.7 Hz), 7.84 (2H, d, J 8.8Hz), 9.88 (1H, s). δ_C ($CDCl_3$): 69.00, 115.00 (2C), 118.37, 130.02, 131.97 (2C), 132.28, 163.60, 190.82.

2.3.2. General procedure for the preparation of p-5-Hexen-1-yloxybenzaldehyde (3b)

The procedure described above in section 2.3.1 was repeated by replacing allyl bromide (2a) with 6-bromo-1-hexene (2b) (20.8 g, 0.13 mol). The reaction was continued in a closed reaction vessel for 12 h at 65 °C and a further 12 h at 90 °C. After the time elapsed, the workup procedure described above was followed; the *p*-hexenyloxybenzaldehyde (3b) was isolated as a brown liquid. ^{1}H NMR spectrum has shown that the product (3b) is very pure, and used without further purification; the yield was 25 g (94%). (Found: C, 76.2; H, 7.8. $C_{13}H_{16}O_2$ requires C, 76.44; H, 7.90%). $\nu_{max.}$ (neat) 3074, 2939, 2868, 2736, 1692, 1640, 1601, 1577, 1509, 1471, 1428, 1394, 1312, 1257, 1216, 1160, 1110, 998, 951, 913, 833, and 650 cm^{-1}. δ_H ($CDCl_3$): 1.59 (2H, quint, J 7.6 Hz), 1.84 (2H, quint, *J* 6.5 Hz), 2.13 (2H, q, *J* 7.0 Hz), 4.05 (2H, t, *J* 6.5 Hz), 5.04 (2H, m), 5.83 (1H, m), 6.98 (2H, d, *J* 8.6 Hz), 7.81 (2H, d, *J* 8.8Hz), 9.87 (1H, s). δ_C ($CDCl_3$): 25.21, 28.48, 33.35, 68.18, 114.74 (2C), 114.93, 129.78, 131.99 (2C), 138.31, 164.20, 190.81.

2.3.3. General procedure for the preparation of p-10-Undecen-1-yloxybenzaldehyde (3c)

The procedure described in section 2.3.1 was repeated with 11-bromo-1-undecene (2c) (30.4 g, 0.13 mol) instead of allyl bromide (2a). The reaction was continued in a closed reaction vessel for 12 h at 65 °C and subsequent 12 h at 90 °C. After the time elapsed, following the similar workup procedure described above, the *p*-10-Undecenyloxybenzaldehyde (3c) was isolated as a brown liquid. ^{1}H NMR spectrum has shown that the product (3c) is very pure, and used without further purification; the yield was 31.4 g (88%). (Found: C, 78.6; H, 9.4. $C_{18}H_{26}O_2$ requires C, 78.79; H, 9.55%). $\nu_{max.}$ (neat) 3074,

2926, 2853, 2733, 1693, 1640, 1601, 1577, 1509, 1467, 1429, 1393, 1311, 1258, 1216, 1160, 1109, 1015, 910, 832, 723 and 617 cm^{-1}. δ_H ($CDCl_3$): 1.20-1.60 (12H, m), 1.83 (2H, quint, *J* 6.8 Hz), 2.03 (2H, q, *J* 7.0 Hz), 4.05 (2H, t, *J* 6.6 Hz), 4.95 (2H, m), 5.82 (1H, m), 6.99 (2H, d, *J* 8.6 Hz), 7.81 (2H, d, *J* 8.8 Hz), 9.87 (1H, s). δ_C ($CDCl_3$): 25.95, 28.91, 29.05, 29.10, 29.32, 29.41, 29.48, 33.80, 68.41, 114.16, 114.75 (2C), 129.74, 131.99 (2C), 139.17, 164.27, 190.80.

2.3.4. Reaction of N-methyl nitrone 4 with p-allyloxybenzaldehyde (3a): Synthesis of adduct p-(2-methylisoxazolidin-5-yl)methyloxybenzaldehyde (5a)

Sodium acetate trihydrate (8.84 g, 65 mmol) was added to a mixture of *N*-methylhydroxylamine hydrochloride (5.00 g, 60 mmol) in ethanol (45 ml), followed by the addition of paraformaldehyde (2.7 g, 90 mmol). The reaction mixture was stirred for 40 min at 65 °C to generate nitrone (4). After the addition of alkene (3a) (10.2 g, 63 mmol) to the nitrone (4), the reaction mixture was heated in a closed vessel at 100 °C for 8 h. Upon completion of the reaction, ethanol was removed. De-ionized water (50 ml) was added to the residual mixture, and subsequently solid $NaHCO_3$ was added to neutralize the solution. The aqueous layer was extracted with ether (3×75 ml). The combined organic layers were dried (Na_2SO_4), concentrated, and the residual liquid was purified by a chromatographic technique, using ether as an eluent to give the product (5a) as a white solid; the yield was 11.6 g (87.4%). Mp 45-46 ºC (ether-hexane), (Found: C, 65.0; H, 6.7; N, 6.2. $C_{12}H_{15}NO_3$ requires C, 65.14; H, 6.83; N, 6.33%). $\nu_{max.}$ (KBr) 2955, 2845, 2739, 1689, 1600, 1578, 1510, 1452, 1429, 1396, 1312, 1258, 1217, 1162, 1111, 1024, 889, and 834 cm^{-1}. δ_H ($CDCl_3$) Slow nitrogen inversion complicates the ^1H NMR spectrum: 2.00-3.00 (6H, m including two N-Me singlets at 2.71 (major) and 2.75 (minor), 3.31 (1H, m), 3.85-4.65 (3H, m), 7.03 (2H, d, *J* 8.6 Hz), 7.82 (2H, d, *J* 8.6 Hz), 9.88 (1H, s). δ_C ($CDCl_3$): The signals of the two invertomers are displayed by the spectrum; the non-overlapping signals for the minor invertomer are written in parentheses: 31.46 (31.72), 44.92 (45.48), 56.48 (56.95), 70.09 (69.56), 74.88 (75.80), 114.90 (2C), 130.07, 131.91 (2C), 163.81, 190.79. The invertomer ratio was estimated to be 67:33.

2.3.5. Reaction of N-methyl nitrone 4 with p-4-butyl-1-yloxybenzaldehyde (3b): Synthesis of adduct 6-p-(2-Methylisoxazolidin-5-yl)hex-1-yloxybenzaldehyde (5b)

The reaction procedure described in section 2.3.4 was repeated by replacing allyl aldehyde (3a) with *p*-5-hexenyloxybenzaldehyde (3b) to give the product (5b) as a colorless solid; the yield was 14.3 g (86%). Mp 36-37 ºC (ether-hexane), (Found: C, 68.2; H, 7.9; N, 5.2. $C_{15}H_{21}NO_3$ requires C, 68.42; H, 8.04; N, 5.32%). $\nu_{max.}$ (KBr) 2945, 2867, 2736, 1691, 1600, 1510, 1465, 1430, 1395, 1311, 1257, 1217, 1161, 1110, 1068, 1023, and 834 cm^{-1}. δ_H ($CDCl_3$) Slow nitrogen inversion complicates the ^1H NMR spectrum: 1.48-2.00 (7H, m), 2.43 (2H, m), 2.65 and 2.70 (3H, N-Me singlets), 3.31 (1H, m), 4.00-4.25 (3H, m), 6.98 (2H, d, *J* 8.9 Hz), 7.82 (2H, d, *J* 8.9 Hz), 9.87 (1H, s). δ_C ($CDCl_3$): The signals of the two invertomers of almost equal intensities are displayed by the spectrum; the non-overlapping signals for the two invertomers are written in parentheses: 22.76, 29.01, (34.30, 34.69), (34.78, 35.08),

(45.19, 45.46), (56.44, 57.12), 68.13, (76.27, 77.85), 114.72 (2C), 129.75, 131.96 (2C), 164.14, 190.78. The invertomers were estimated to be in a ratio of 1:1.

2.3.6. Reaction of N-methyl nitrone 4 with p-10-undecen-1-yloxybenzaldehyde (3c): Synthesis of adduct p-9-(2-Methylisoxazolidin-5-yl)undec-1-yloxybenzaldehyde (5c)

The reaction procedure described in section 2.3.4 was repeated using *p*-10-undecen-1-yloxybenzaldehyde (3c) instead of allyl aldehyde (3a) to give the product (5c) as a colorless solid; the yield was 18.9 g (90%). Mp 52-53 ºC (ether-hexane), (Found: C, 71.9; H, 9.2; N, 4.1. $C_{20}H_{31}NO_3$ requires C, 72.04; H, 9.37; N, 4.20%). $\nu_{max.}$ (KBr) 2928, 2854, 2734, 1693, 1601, 1577, 1509, 1466, 1430, 1394, 1312, 1258, 1216, 1160, 1113, 1016, 834, and 731 cm^{-1}. δ_H ($CDCl_3$) Slow nitrogen inversion complicates the ^1H NMR spectrum: 1.20-1.90 (17H, m), 2.00-2.72 (5H, m including two N-Me singlets at 2.64 and 2.70), 3.25 (1H, m), 3.95 and 4.16 (1H, two multiplets for the two invertomers), 4.03 (2H, t, *J* 6.5 Hz), 6.98 (2H, d, *J* 8.8 Hz), 7.82 (2H, d, *J* 8.8 Hz), 9.87 (1H, s). δ_C ($CDCl_3$): The signals of the two invertomers are displayed by the spectrum; the non-overlapping signals for the minor invertomer are written in parentheses: 25.92, 26.21, 29.04, 29.29, 29.43 (2C), 29.60, 34.78 (34.25), 35.05 (35.41), 45.46 (45.21), 57.16 (56.44), 68.40, 78.15 (76.52), 114.74 (2C), 129.73, 131.98 (2C), 164.26, 190.79. The invertomer ratio was estimated to be 55:45.

2.3.7. Preparation of the nitrone 1-pyrroline 1-oxide (6)

The nitrone 1-pyrroline 1-oxide (6) was prepared following a previously published procedure found in the literature [39].

2.3.8. Reaction of nitrone 6 with undecenyloxy aldehyde 3c: Synthesis of adduct p-9-[hexahydropyrrolo(1,2-b)isoxazol-2-yl]nonyloxybenzaldehyde (7)

A solution of the nitrone (6) (30 mmol) and the alkene (3c) (11.0 g, 40 mmol) in toluene (75 ml) was refluxed for 6 h under N_2. After the time elapsed, the solvent was removed from the reaction mixture, and then the residual mixture was purified by a chromatographic technique using ether and methanol (98:2 v/v) as an eluent to give the product (7) as a solid; the yield was 8.2 g (76%). Mp 57-58 ºC (ether), (Found: C, 73.4; H, 9.3; N, 3.8. $C_{22}H_{33}NO_3$ requires C, 73.50; H, 9.25; N, 3.90%). $\nu_{max.}$ (KBr) 2931, 2855, 2716, 1690, 1599, 1508, 1464, 1386, 1311, 1251, 1213, 1157, 1111, 1010, 842, and 725 cm^{-1}. δ_H ($CDCl_3$): 1.20-2.10 (22H, m), 3.15 (2H, m), 3.75 (1H, m), 4.04 (3H, m), 6.98 (2H, d, *J* 8.6 Hz), 7.83 (2H, d, *J* 8.8 Hz), 9.87 (1H, s). δ_C ($CDCl_3$): 24.15, 25.79, 26.22, 28.82, 28.99, 29.14, 29.23, 29.41, 31.54, 33.78, 42.29, 56.93, 64.71, 68.18, 76.37, 114.53 (2C), 129.49, 131.77 (2C), 164.04, 190.57.

2.4. Specimens

The mild steel coupons having the composition of 0.089% (C), 0.34% (Mn), 0.037 (Cr), 0.022 (Ni), 0.007 (Mo), 0.005 (Cu), 0.005 (V), 0.010 (P), 99.47% (Fe) were used to study the corrosion inhibition by gravimetric and electrochemical measurements in a 1 M HCl, 0.5 M H_2SO_4 and CO_2-saturated 0.5 M NaCl solution. Flag-shaped mild steel specimens (thickness: 1 mm, exposed area: 2 cm^2), used for the electrochemical measurements, were abraded with increasing grades of emery papers, then degreased with acetone, washed with de-ionized water, and then again washed with acetone. The specimens were dried and kept in a desiccator. Prior to use, an ultrasonic bath was used to treat the specimens for 5 min, followed by washing with de-ionized water.

For autoclave tests the two types of mild steel coupons, measuring ≈2.5×2.0×0.1 cm^3, have the following composition (in wt%):

Coupon A: 0.082% (C), 0.207% (Mn), 0.016% (Cr), 0.062% (Ni), 0.012% (Mo), 0.029% (Cu), <0.001% (V), <0.0005% (P), 0.032% (Si), 0.0059% (S), 0.045% (Al), 0.011% (Co), <0.0005% (Ti), <0.0010 (Nb), <99.3% (Fe).

Coupon B: 0.168% (C), 0.495% (Mn), 0.038% (Cr), 0.034% (Ni), 0.0081% (Mo), 0.074% (Cu), 0.001% (V), 0.014% (P), 0.237% (Si), 0.024% (S), 0.080% (Al), 0.011% (Co), 0.0015% (Ti), 0.0019 (Nb), <98.6% (Fe).

2.5. Solutions

HCl and H_2SO_4 solutions were prepared from reagent grade HCl and H_2SO_4 by diluting to 1.0 M or 0.5 M, with distilled de-ionized water. Corrosion inhibition tests were performed in 0.5 M NaCl in two different environments in the presence of (a) CO_2 (1 atm) at 40 ºC, and (b) higher pressure (10 bar ≈ 9.9 atm) of CO_2 at higher temperature (120 ºC). De-aeration of the solution was performed with 99.999% N_2 for 30 min and then the solution underwent continuous saturation with 99.999 % pure CO_2 to prevent any corrosion by oxygen. The corrosion studies using CO_2 have shown that the corrosion at pH < 4 occurs mainly due to the reaction with H^+, while the active species in less acidic solutions adsorbed CO_2 or carbonic acid (H_2CO_3) [40]. The $NaHCO_3$ (100 mg L^{-1}) solution was used to maintain the pH of the test solution in between 5.0 and 5.5 to avoid potential alterations in the mechanism of the corrosion reaction.

2.6. Gravimetric measurements

2.6.1. Gravimetric measurements in 1 M HCl and 0.5 M H_2SO_4 at 60 ºC, CO_2-saturated 0.5 M NaCl (1 atm) at 40 ºC

For gravimetric measurements, steel coupons with a dimension of 2.5×2.0×0.1 cm^3, were used. The inhibition study in 1 M HCl and 0.5 M H_2SO_4 was carried out at 60 ºC by hanging the mild steel coupon for an immersion time of 6 h using acid solutions of 250 ml in the absence or presence of the synthesized inhibitors. After the time elapsed, the coupons were wiped with tissue paper, lightly polished with emery paper, followed by a washing with de-ionized water and acetone, and dried at 110

ºC for 6 h. A similar procedure described as above was used to determine the corrosion efficiency of the synthesized inhibitors in CO_2-saturated 0.5 M NaCl (1 atm) for an immersion time of 7 days at 40 ºC. Each measurement was carried out three times, with each of the inhibitors, and with solutions containing no inhibitor in order to check the reproducibility. Steel coupons having an almost equal size and masses were used in all measurements. The relative weight losses of the coupons were used to calculate the percent inhibition efficiency (η %), using Eq. (1):

$$\eta\ \% = \frac{\text{Wb - Wi}}{\text{Wb}} \times 100 \quad (1)$$

where, Wb and Wi represent weight loss in the absence or presence of an inhibitor, respectively.

2.6.2. Gravimetric measurements at high temperature and pressure

The synthesized inhibitors were tested at elevated temperatures (120 ºC) and pressure (9.9 atm) in 0.5 M NaCl solution saturated with CO_2 that approximate the conditions present in oil and gas field applications. Experiments were conducted using a microcomputer attached to an Autoclave, which was intended to test inhibitor samples at a pressure up to 413 bar(g) and temperature of 648 ºC with a volume capacity of 1000 ml. The autoclave was equipped with a temperature probe, pressure transducer, sparger and a cooling coil. All accessories were designed to match the pressure and temperature ratings. The vessel was mounted on a hoisting mechanism that helped in removing the cover conveniently, despite its heavy weight. An electrically heated jacket was used to heat the autoclave. The temperature inside the reactor was controlled by a feedback PID controller. The user could specify the set-point of the temperature and other PID parameters via SCADA software. The test solution was 0.5 M NaCl solution prepared from double distilled water. A predetermined quantity of the inhibitor was dissolved in the solution, and the solution (50 ml) was transferred into a temperature resistant glass liner that was kept in the autoclave. CO_2 was passed through the solution for 20 minutes, steel coupons were placed in the solution, and then the autoclave was closed. CO_2 gas was used to pressurize the autoclave up to the desired level. The solution temperature was controlled within a range of ±2 ºC. The entire duration of the experiment (48 h) was set to have the temperature and pressure monitored by the PID controller. Each measurement was carried out three times in order to check the reproducibility.

2.7. Polarization measurements

The potentiodynamic polarization studies were carried out in 250 ml of 1 M HCl at 60 ºC or CO_2-saturated 0.5 M NaCl solution (1 atm) containing inhibitors at 40 ºC. The experiments were performed in a 750 ml round-bottom flask fitted with a mild steel working electrode, saturated calomel electrode (SCE), and a counter graphite electrode. After connecting all three electrode cells to the potentiostat, the polarization curves were recorded by a computer-controlled potentiostat-galvanostat (Auto Lab, Booster 10A-BST707A, Eco Chemie, Netherlands) where the cutoff current was set at 10 mA. A computer (Windows 7) loaded with NOVA (Version 1.8) software processed the data. The

working electrode was pre-corroded until a stable open circuit potential (OCP) was achieved, usually within the exposure time of 30 min, after which a scan of ± 250 mV with respect to the OCP was conducted at a rate of 0.5 mV s^{-1}. After carefully analysing individual Tafel plots, the current density (i_{corr}) and corrosion potential (E_{corr}) were determined from the respective media.

The Linear Polarization Resistance (LPR) measurements were carried out using the same cell described above. The η % from the LPR technique was calculated using Eq. (2):

$$\eta\% = \left(\frac{R'_p - R_p}{R'_p}\right) \times 100 \quad (2)$$

where R_p and R'_p represents the polarization resistance in the absence or presence of inhibitors.

The polarization resistance with a range of ±10 mV around E_{corr} was scanned to obtain the current potential plots, which were used to attain the polarization resistance.

2.8. Electrochemical Impedance Spectroscopy (EIS)

The impedance measurements were carried out in a 750 ml round-bottom flask fitted with a three electrodes system, as described above in section 2.7. A solution of 0.5 M NaCl (250 ml), containing 100 mg L^{-1} $NaHCO_3$, was saturated with CO_2 (1 atm) at 40 ºC and was used as a test solution. The impedance plots were recorded using a computer-controlled potentiostat-galvanostat (Auto Lab, Booster 10A-BST707A). The impedance measurements were carried out at the OCP with a frequency scan ranging from 100 KHz to 50 mHz, and with an amplitude value of 10 mV. The impedance curves were plotted, and the electrochemical equivalent circuit parameters obtained, by fitting the data using NOVA (Version 1.8) software.

2.9. Surface tension

The surface tensions of the inhibitors in the CO_2-saturated 0.5 M NaCl solution at 40 ºC were measured by a PHYWE surface tensiometer equipped with a torsion dynamometer (0.01 N) and platinum iridium ring (1.88 cm diameter) (Germany), as described in previously published literature [41].

2.10. The standard free energy of micelle formation ($\Delta G°_{mic}$)

The $\Delta G°_{mic}$ of the synthesized inhibitors is given by Eq. (3) [39],

$$\Delta G°_{mic} = RT \ln(C_{cmc}) \quad (3)$$

where R, T and C_{cmc} represent the gas constant, temperature and inhibitor concentration in mol L^{-1} at the critical micelle concentration (CMC).

3. RESULTS AND DISCUSSION

3.1. Synthesis of the corrosion inhibitors

A nitrone-alkene cycloaddition protocol was used for the synthesis of the corrosion inhibitor molecules, which is indeed the most promising chemical protocol [42] for the preparation of the

isoxazolidine derivatives (Fig. 1). The nitrone-cycloaddition reactions play a significant role in the synthesis of many biologically important natural products [43].

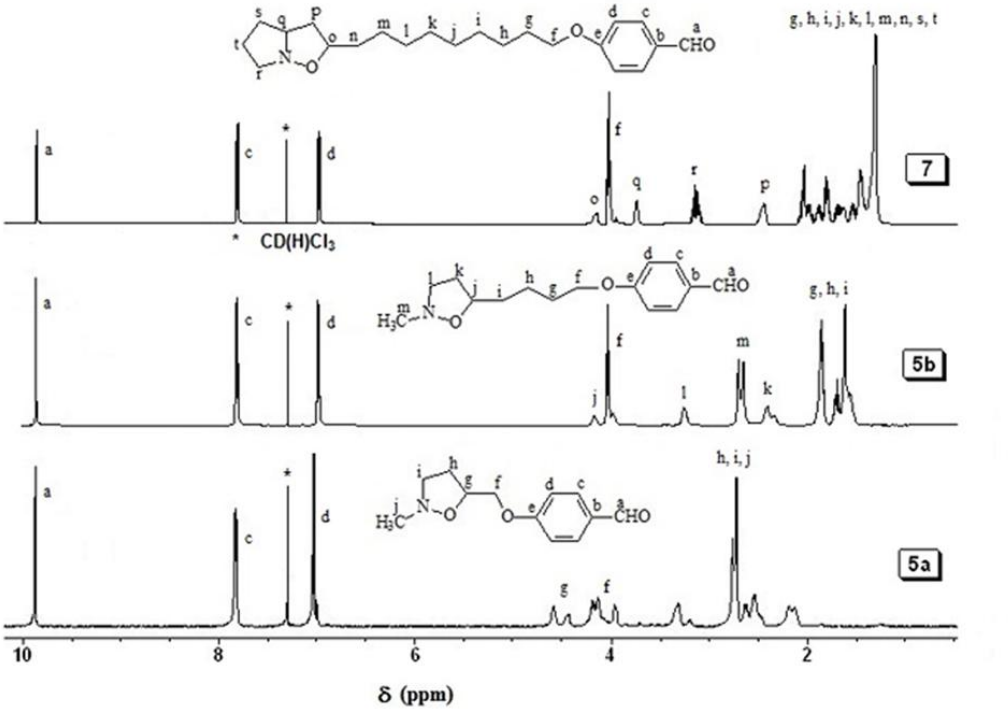

Figure 2. ^{1}H NMR spectra of **5a**, **5b** and **7** in $CDCl_3$.

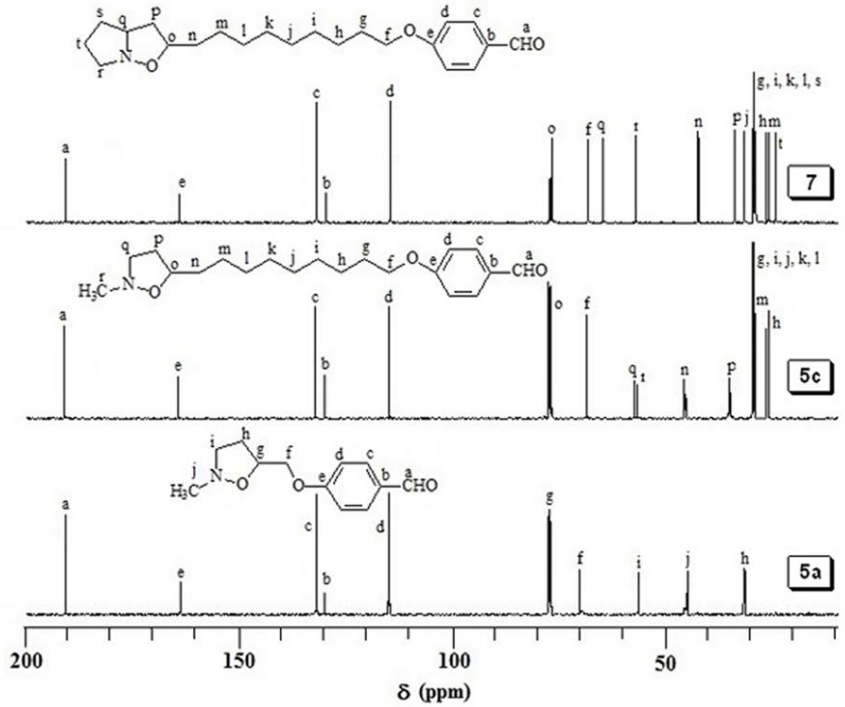

Figure 3. ^{13}C NMR spectra of **5a**, **5c** and **7** in $CDCl_3$.

A new class of inhibitor molecules containing N, O and with variable chain lengths of hydrophobe with an alkyl group or aliphatic bicyclic ring, as well as aldehyde moiety, was synthesized (Fig. 1). The specialty alkenes (3a), (3b), (3c), having variable chain lengths of alkyloxy functionality, were prepared via alkylation of *p*-hydroxybenzaldehyde (1) with bromo alkenes (2). The cycloaddition of acyclic nitrone (4) with (3a), (3b) and (3c) afforded the cycloadducts (5a), (5b) and (5c), respectively, with excellent yields. Likewise, the cycloaddition of nitrone (6) with (3c) gave the adduct (7), an excellent yield. This is expected to make the isoxazolidine moiety in (5) and (7) a potent motifs for chemisorption by nucleophilic electron donation to the metal surface. The ^{1}H and ^{13}C NMR spectra of some of these interesting inhibitor molecules (5) and (7), are displayed in Fig. 2 and 3, respectively. The characteristic Hs marked a, b, and c are readily identifiable in the proton spectra. Aromatic Hs appeared at the expected places with the anticipated multiplicities.

Two commercial inhibitor samples were tested for the sake of comparison. QI80-E, from Materials Performance, is an ethylsulfate Quaternized Imidazoline (a mixture having R = C_{12} to C_{22}), used for sweet corrosion, to a certain limit. ARMOHIB 219, from AKZO NOBEL, is an imidazoline based on oleic acid and diethylenetriamine (Fig. 1).

3.2. Gravimetric measurements

3.2.1. Measurements in 1 M HCl, 0.5 M H_2SO_4, and CO_2-saturated 0.5 M NaCl at 1 atm

The results of weight loss measurements at 60 ºC after 6 h of immersion of the steel coupons for the synthesized compounds in 1 M HCl or 0.5 M H_2SO_4 are reported in Tables 1 and 2. The steel coupons' results, which were immersed for 7 days at 40 °C in the synthesized compounds containing CO_2-saturated 0.5 M NaCl solution at 1 atm, are reported in Table 3. The average weight losses in percentage, reported in the Table 1, 2 and 3 are deviated within a range of 0.5-2.5%.

Table 1. The η %[a] for different inhibitors for the inhibition of corrosion of mild steel exposed at 60 ºC in 1 M HCl (6 h).

Concentration (ppm)	η (%) for inhibitor compounds in 1 M HCl			
	5a	5b	5c	7
1	12.6	19.3	27.8	42.9
3	28.3	46.2	53.8	75.8
5	37.0	50.8	67.9	79.4
10	45.2	60.9	94.6	97.3
20	57.1	69.1	95.2	99.1
50	70.1	80.7	98.5	99.4
100	78.3	88.7	98.1	99.5
200	81.8	92.4	99.3	99.8

[a] Inhibition Efficiency, IE (i.e., η) = surface coverage θ.
[b] The blank was 1 M HCl.
[c] Inhibitor sample was dissolved in 250.0 ml 1 M HCl solution

Table 2. The η %[a] for different inhibitors for the inhibition of corrosion of mild steel exposed at 60 ºC in 0.5 M H_2SO_4 (6 h).

Concentration (ppm)	η (%)			
	5a	5b	5c	7
1	1.21	1.61	2.53	3.72
3	7.91	9.10	13.8	16.3
5	12.5	16.3	19.7	22.5
10	18.3	24.7	31.8	36.8
20	27.2	32.7	44.7	60.9
50	36.7	43.8	59.7	67.7
100	43.8	52.3	76.1	79.2
200	50.9	64.2	87.3	92.6

[a] Inhibition Efficiency, IE (i.e., η) = surface coverage θ.
[b] The blank was 0.5 M H_2SO_4.
[c] Inhibitor sample was dissolved in 250.0 ml in 0.5 M H_2SO_4 solution.

Table 3. Corrosion inhibition efficiency, η (%) using polarization resistance, Tafel plots and gravimetric method of mild steel samples in various solutions containing 20, 50 and 100 ppm by weight of the inhibitors in 0.5 M NaCl solution saturated with CO_2 (1 atm) at 40 ºC.

Compound	η (%)						
	Polarization Resistance			Tafel method			Gravimetric method
	20[a]	50[a]	100[a]	20[a]	50[a]	100[a]	100[a]
5a	67.2	73.8	80.9	62.7	69.6	77.3	81.1
5b	71.9	78.3	83.8	70.5	76.7	82.1	86.3
5c	83.2	87.3	92.1	79.6	85.4	90.4	93.8
7	97.4	98.1	99.4	97.0	98.3	98.6	98.3

[a]Inhibitor concentration in ppm by weight

The results of corrosion inhibition tests for the new series of isoxazolidines containing a *p*-alkyloxybenzaldehyde moiety in 1 M HCl at 60 °C, using the weight loss method, are presented in Table 1. All the inhibitor molecules 5a-c and 7 demonstrated excellent η % in 1 M HCl at 60 ºC as determined by the gravimetric method. It is evident from Table 1 that the η % value increases with an increase in the inhibitor concentrations, and reached a maximum value which indicates the formation of a monolayer film on to the mild steel coupon surface. In the presence of 100 ppm inhibitors, the gravimetric study revealed η % values 78.3, 88.7, 98.1 and 99.3, while for 20 ppm, the corresponding values were found to be 57.1, 69.1, 95.2 and 99.1 for the compounds 5a, 5b, 5c and 7, respectively (Table 1). In all the concentrations studied, the inhibitor molecule 7 gave the best protection. At a concentration of 20 ppm, the compound 7 was found to be the η % of ≈ 99%. The excellent performance ascertains the efficacy of the functional motifs in the inhibitor molecules to arrest mild steel corrosion.

These synthesized isoxazolidine compounds were also evaluated in 0.5 M H_2SO_4 using the weight loss method. To our satisfaction, the synthesized compounds, particularly 5c and 7, showed very good inhibition efficacies (Table 2). It is worthwhile to mention that the literature does not document many compounds, which are equally effective in arresting mild steel corrosion, both in HCl and in H_2SO_4 media.

3.2.2. Measurements in CO_2-saturated 0.5 M NaCl at high temperature and pressure

The synthesized inhibitor compounds and two commercial samples (QI80-E and ARMOHIB 219), used to determine the inhibition efficiencies at a temperature of 120 °C and a pressure of 9.9 atm CO_2 in 0.5 M NaCl for 48 h, are given in Table 4.

The different elemental compositions and carbon content contained in the two metal coupons A and B were used to determine the percent inhibition efficiencies in 0.5 M NaCl saturated with a pressure of 9.9 atm CO_2 at a temperature of 120 ºC.

Table 4. Corrosion rates and inhibition efficiencies of various corrosion inhibitors (200 ppm) at 120 ºC and 10 bar pressure of CO_2 in 0.5 M NaCl solution.

Solution	Coupon[a]	% Inhibition	Average% Inhibition
BLANK	A	–	–
	B	–	
5a	A	58.1	57.7
	B	57.4	
5b	A	68.5	68.9
	B	69.3	
5c	A	78.5	79.2
	B	79.8	
7	A	85.9	86.3
	B	86.7	
Q I 80	A	80.4	81.0
	B	81.6	
ARMOHIB219	A	81.9	82.7
	B	83.5	

[a] Two mild steel coupons A and B having different carbon content and compositions.

The inhibitor molecules performed very well at high temperature (120 °C) and pressure (9.9 atm, CO_2) to arrest corrosion in 0.5 M NaCl (Table 4). The η % in CO_2-0.5 M NaCl at high temperature and pressure revealed that 7 performed better than 5 in arresting corrosion, as determined using the two types of metal coupons A and B having different elemental compositions and carbon content. To our great satisfaction, the synthesized inhibitor 7 imparted better protection than the two commercial inhibitors QI80 and ARMOHIB219 (Table 4).

3.3. Polarization measurements

In this study, the effect of the immersion time on the OCP versus the SCE in CO_2-saturated 0.5 M NaCl solution was explored for the mild steel coupon in the absence (blank) or presence of different concentrations (1 and 100 ppm) of 5c and 7 at 40 °C. The results obtained for the variation of OCP with time are depicted in Fig. 4.

Table 5. Results of Tafel plots in solutions containing 20 ppm of the inhibitor in 1 M HCl at 60 ºC.

Sample	Tafel plots					Polarization Resistance	
	E_{corr} vs *SCE* (mV)	β_a (mV/dec)	β_c (mV/dec)	i_{corr} (μA cm^{-2})	η (%)[b]	R_p (Ω cm^2)	η (%)[b]
Blank[a]	−459	39.6	94.5	746	–	29.3	–
5a	−440	56.4	114.8	286	61.7	116	74.7
5b	−427	38.6	103.3	182	75.6	170	82.8
5c	−407	54.2	107.1	75.3	89.9	333	91.2
7	−399	47.1	89.4	11.9	98.4	1395	97.9

[a] The blank was a 1 M HCl solution.
[b] Inhibition Efficiency (i.e., η) = Surface coverage θ.

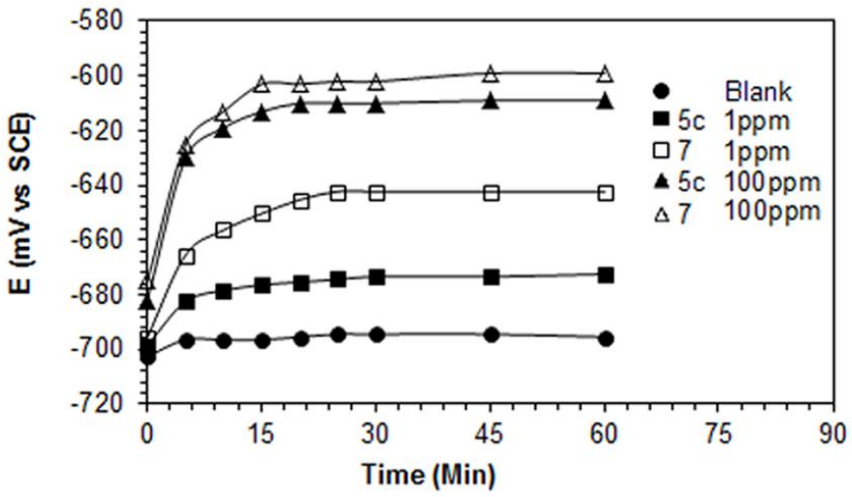

Figure 4. Variation of OCP of mild steel with time of immersion in CO_2-saturated 0.5 M NaCl containing different concentrations (1 and 100 ppm) of **5c** and **7** at 40 ºC.

Table 6. Results of Tafel plots of a mild steel sample in various solutions containing inhibitors **5** and **7** in 0.5 M NaCl saturated with CO_2 at 40 °C.

Sample	Concentration. (ppm)	Tafel plots					LPR[d]
		E_{corr} vs. *SCE* (mV)	β_a (mV/dec)	β_C (mV/dec)	i_{corr} (μA cm^{-2})	η (%)[a]	θ (%)[a]
Blank[b]	0	−704	56.8	−226	126	–	
5a[c]	1	−692	37.7	−178	68.2	45.9	49.2
	5	−683	56.1	−165	57.8	54.1	56.6
	10	−675	49.2	−192	53.9	57.2	59.9
	20	−667	29.5	−225	47.1	62.6	67.2
	50	−656	33.0	−234	38.3	69.6	73.8
	100	−648	48.1	−184	28.6	77.3	80.9
	200	−632	37.9	−169	19.0	84.9	87.5
5b[c]	1	−691	49.2	−213	55.2	56.2	57.6
	5	−678	52.1	−227	48.8	61.3	62.1
	10	−671	57.8	−156	43.1	65.8	67.2
	20	−663	28.3	−179	37.2	70.5	71.9
	50	−650	22.1	−211	29.4	76.7	78.3
	100	−630	26.4	−219	22.6	82.1	83.8

	200	−615	34.1	−194	14.6	88.4	89.9
5c[c]	1	−674	42.7	−189	58.2	53.8	57.4
	5	-649	47.1	−223	45.1	64.2	69.4
	10	-642	56.3	−213	36.7	70.9	75.1
	20	−631	23.1	−189	25.7	79.6	83.2
	50	−619	47.3	−226	18.4	85.4	87.3
	100	−605	21.8	−217	12.1	90.4	92.1
	200	−590	43.6	−239	7.19	94.3	95.5
7[c]	1	−681	34.5	−203	47.8	62.1	63.3
	5	−668	58.1	−190	29.5	76.6	78.1
	10	−640	41.9	−217	22.2	82.4	84.6
	20	−619	46.2	−194	3.78	97.0	97.4
	50	−609	23.9	−215	1.51	98.8	98.1
	100	−598	27.3	−221	1.76	98.6	99.4
	200	−586	38.1	−223	1.13	99.1	99.6

[a] Inhibition Efficiency (i.e., η) = surface coverage θ.
[b] The blank was a 0.2% v/v 2- propanol in 0.5 M NaCl solution saturated with CO_2.
[c] The inhibitor sample was dissolved in 0.5 ml 2-propanol, and added with 249.5 ml blank solution.
[d] Polarization resistance for blank: 108 Ω cm^2

For a blank solution, the OCP changed very quickly towards a less negative value and became stable, corresponding to the free corrosion potential, E_{corr}, of the metal. However, in the presence of inhibitors, E_{corr} shifted to the less negative direction and became stable after 20 min. The magnitude of the E_{corr} shifts increased with the increase in the inhibitor concentration. The E_{corr} shift to the more noble direction is attributed to the preferential adsorption of the inhibitors on the anodic sites of the mild steel surface.

The Tafel extrapolation plots and linear polarization resistance method were used to determine the corrosion inhibition efficiencies of mild steel using synthesized inhibitor compounds in 1 M HCl at 60 ºC, or CO_2-saturated 0.5 M NaCl solution at 40 ºC. These results are summarized in Tables 5 and 6. Some representative Tafel plots for the inhibition in 1 M HCl and in CO_2-saturated 0.5 M NaCl are shown in Fig. 5 and 6, respectively. The results of the weight loss method (Table 1) was reconfirmed from the outcomes of the η % of the synthesized compounds (20 ppm) in 1 M HCl by Tafel extrapolations (Table 5). The inhibitive nature of the synthesized molecules was confirmed as the i_{corr} values are remarkably decreased. In the presence of the inhibitor molecules, the E_{corr} values have shifted to a less negative direction of 1 M HCl, suggesting that the synthesized molecules are an anodic type of inhibitor, which mainly suppresses the anodic reaction. In the presence of an inhibitor, the shifting of the OCP by at least 85 mV can be considered either as a cathodic or anodic type inhibitor [44]. The shifting of 20 to 60 mV (Table 5) towards the less negative direction is not significantly important for the molecules to be classified as anodic type inhibitors. The higher reduction in the anodic current densities is indicative of the greater decrease in the anodic oxidation rate compared to the rate of hydrogen evolution in the cathodic reaction. Under the major influence of anodic control, the inhibitors behave like the mixed inhibitors; they formed a barrier film on the metal surface instead of prompting the corrosion reactions, as indicated by the decreased values of the cathodic (β_c) and anodic (β_a) slopes.

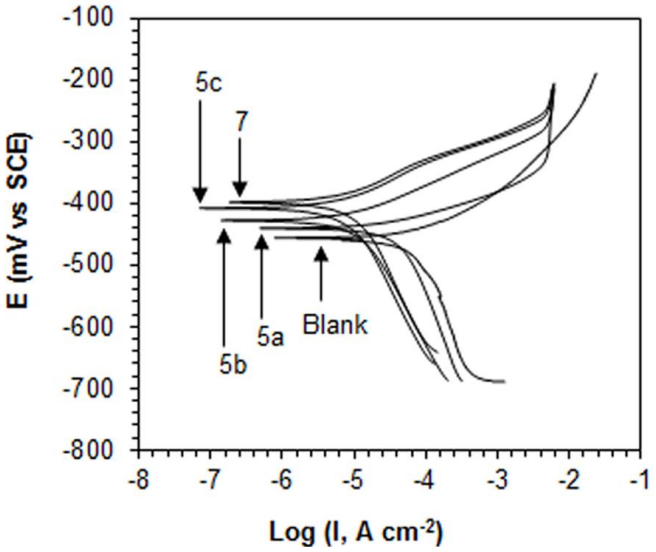

Figure 5. Potentiodynamic polarization curves at 60 ºC for mild steel in 1 M HCl containing 20 ppm of **5** and **7**.

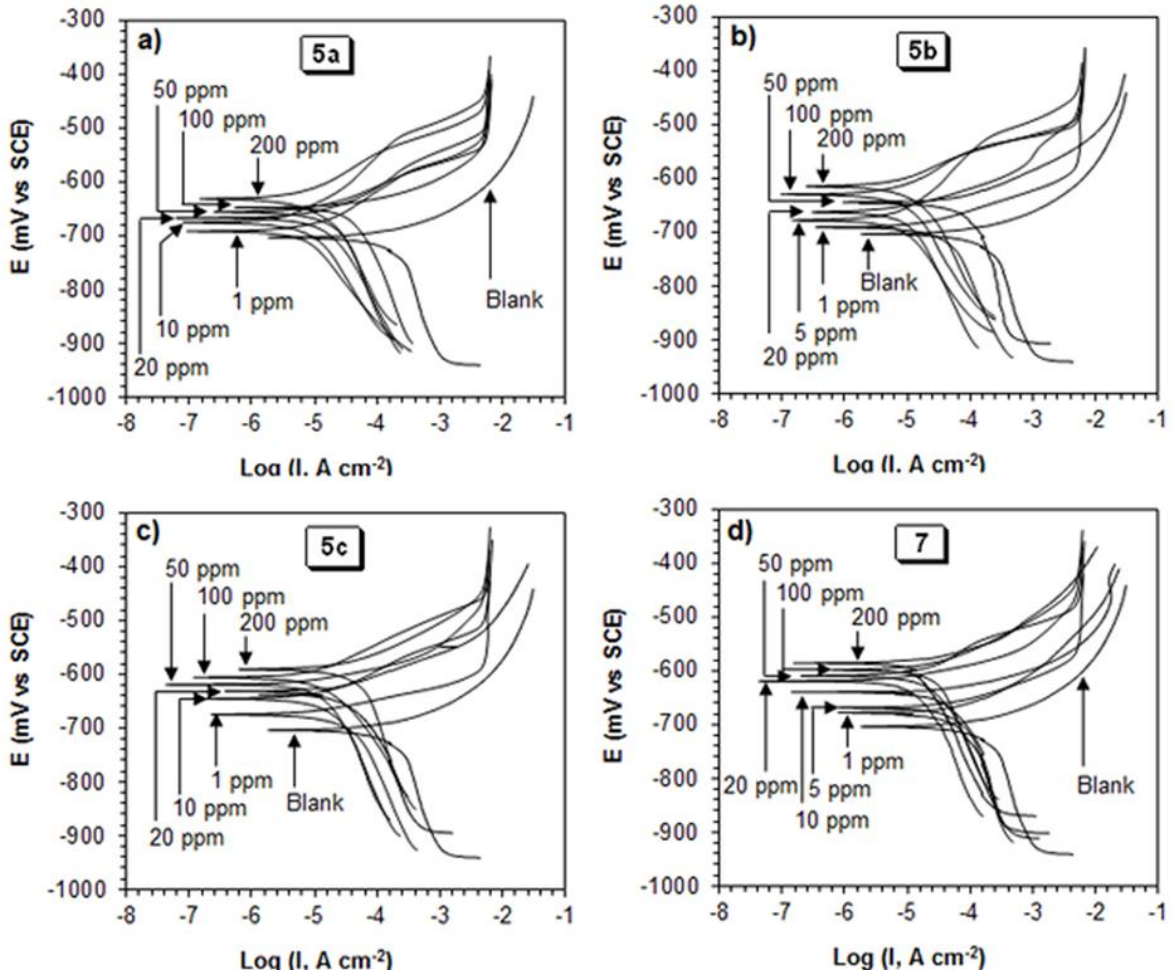

Figure 6. Potentiodynamic polarization curves at 40 ºC for mild steel in CO_2-saturated 0.5 M NaCl containing different concentrations of **5** and **7**.

The advantageous role of the π- and non-bonded electrons, and the hydrophobic alkyl chain, may be augmented by the very high η %. On the anodic sites, the adsorption of the inhibitor molecules are assisted by these polarizable electrons through their interaction with the d-orbitals of iron or Fe^{2+}.

We investigated the corrosion inhibition efficiencies of the synthesized inhibitor molecules in CO_2-saturated 0.5 M NaCl. Table 3 establishes the comparison between the η % attained from weight loss measurements at 40 °C after 7 days of immersion in the existence of 100 ppm of the inhibitor molecules, and η %, obtained from Tafel extrapolation and linear polarization resistance at 40 °C. To our great satisfaction, the inhibitor compounds 5c and 7 showed excellent inhibition efficiencies. The outcomes obtained from the gravimetric method (Table 3) which is currently the simplest and most consistent technique, were confirmed by the Tafel and LPR data.

Table 6 presents the results obtained from the Tafel extrapolation and LPR in the presence of various concentrations (1-200 ppm) of the inhibitors 5 and 7 in CO_2-saturated 0.5 M NaCl at 40 ºC. As evident from Table 6 and Fig. 6, the inhibitor compounds suppressed mainly the anodic reactions as the E_{corr} values shifted more and more to less negative values with increasing inhibitor concentrations. In the presence of 100 ppm of inhibitor, the E_{corr} values shifted in the range 50-120 mV do not qualify all these inhibitors to be classified under the anodic type; a shift of at least 85 mV is suggested to be a requirement for an inhibitor to be classified as either a cathodic or anodic type [44]. Nonetheless, the compounds 5b, 5c and 7 can be classified as anodic type inhibitors [45]. It is evident from Fig. 6 that the presence of the inhibitors causes a much greater reduction in the i_{corr} in the anodic than the cathodic branch. Inhibitor action is thus more pronounced in mitigating the iron dissolution at the anode than the cathodic reaction for hydrogen evolution. The inhibitor compounds in the current work are thus considered as mixed-type inhibitors under the predominance of anodic control. The addition of inhibitors did not change the mechanism of the electrode reactions since the slopes of β_c and β_a are not changed considerably; the inhibitors simply block the anodic and cathodic reaction sites.

In Fig. 6, most of the anodic polarization curves in the current-versus potential plots display desorption potentials, which can be explained by the presence of current-increasing plateaus [46]. The presence of a desorption potential anticipates a pathway in which the inhibitors initially arrest the anodic sites on the electrode and desorb at a higher potential, leading to enhanced steel dissolution.

3.4. Impedance measurements

The Nyquist plots of the solution-mild steel interface were obtained in the absence or presence of inhibitors 5c and 7 by the Randles electrochemical equivalent circuit, depicted in Fig. 7. The fitted electrochemical equivalent circuit shown in Fig. 7 contains a solution resistance (R_s), polarization resistance (R_p) and constant phase element (CPE). The R_s, obtained from crossing the semicircle with the real part (Z') axis at high frequency, is the potential drop between the mild steel electrode and the reference electrode. The R_p consists of a charge transfer resistance and a diffusion layer resistance at the surface of the mild steel electrode [47]. The polarization resistance at the mild steel electrode's surface R'_p can be calculated using Eq. (4).

$$R'_p = R_p - R_s \quad (4)$$

The corrosion resistance in the absence (blank) or presence of an inhibitor solution will be used to determine the corrosion inhibition efficiency of the inhibitor.

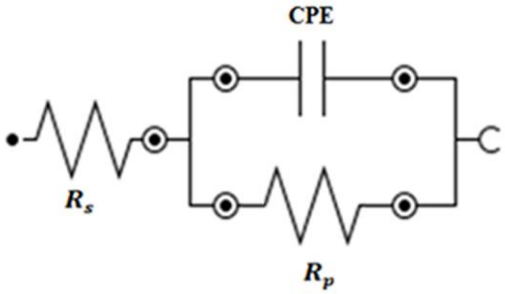

Figure 7. Randles electrochemical equivalent circuit diagram used for modeling metal/solution interface. R_s: Solution resistance, R_p: Polarization resistance, CPE: Constant phase element.

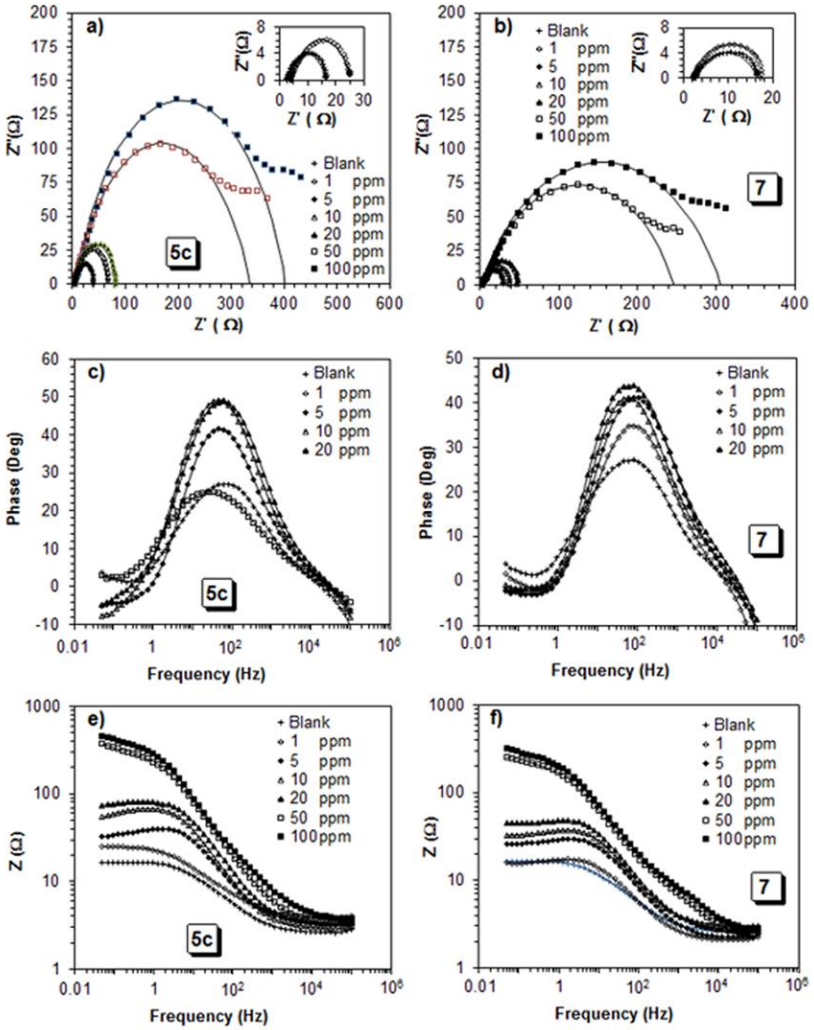

Figure 8. Nyquist diagram of (a) **5c** and (b) **7**, Bode phase angle plots of (c) **5c** and (d) **7**, and impedance plots (e) **5c** and (f) **7** of mild steel at 40 ºC in CO_2-saturated 0.5 M NaCl containing various concentrations of inhibitors in 30 minutes immersion time**.** Various symbols represent experimental data and solid lines in the Nyquist plot represent fitted data.

The double layer capacitance and coating capacitance modeled with a CPE depends on a degree of surface homogeneity (n) of the uninhibited and inhibited mild steel surface [48]. Due to inadequate homogeneity of the surface, the n value in Eq. (5) is lower than 1 and the symbol *Q* was used in place of capacitance (c).

$$Z = \frac{1}{(\mathrm{i}\omega \mathrm{Q})\mathrm{n}} \quad (5)$$

where *Z* represents the imaginary part, ω is the frequency (radian) and *i* is the current (A).

For a better understanding of mild steel corrosion inhibition, EIS measurements were performed to investigate the influence of different concentrations of 5c and 7 in CO_2-saturated 0.5 M NaCl at 40 °C. (Fig. 8a, b). Fig. 8a and 8b display the Nyquist plots in the absence or presence of various concentrations (1-100 ppm) of inhibitors 5c and 7.

The inset figures (Fig. 8a, b) depict magnified forms of Nyquist plots in the absence or presence of 1 ppm inhibitor. The diameter of the impedance semicircle increases with an increase in the concentrations of the inhibitors, which implies an increase in the inhibitors on the mild steel surface, and thus an increase in the resistivity of the electrode. The figures demonstrate that the Nyquist diagrams do not maintain a perfect semicircle; therefore the capacitance at the inhibitor solution-metal interface does not exhibit the properties of a real capacitor. The non-ideal or depressed semicircle in the Nyquist plots obtained at a high to medium frequency is characteristic to the solution-solid electrode interface that is associated with the physical properties, such as surface roughness and inhomogeneity of the electrode [49].

Table 7. Impedance parameters for the corrosion of a mild steel sample in various solutions containing inhibitors **5c** and **7** in CO_2 -0.5 M NaCl at 40 ºC.

Sample	Concentration (ppm by weight)	R_s (Ω cm^2)	R_p (Ω cm^2)	CPE[a] (μF cm^{-2})	n	R'_p (Ω cm^2)	η (%)
Blank		4.19	18.7	699	0.963	14.5	
5c	1	3.57	36.9	473	0.971	33.3	56.4
	5	3.51	51.7	245	0.965	48.2	69.9
	10	3.31	67.2	334	0.945	63.9	77.3
	20	3.86	107	266	0.932	103	85.9
	50	4.63	127	285	0.919	122	88.1
	100	6.49	219	246	0.812	213	93.2
7	1	2.12	42.3	553	0.961	40.2	63.9
	5	2.30	70.4	327	0.895	68.1	78.7
	10	3.09	93.2	313	0.879	90.1	83.9
	20	2.82	486	276	0.747	483	97.0
	50	2.66	662	379	0.719	659	97.8
	100	2.64	969	336	0.703	966	98.5

[a]Double layer capacitance (C_{id}) and coating capacitance (C_c) are usually modelled with a constant phase element (CPE) in modeling an electrochemical phenomenon.

At higher inhibitor concentrations (50 and 100 ppm), the shape of the semicircle of the Nyquist plots (Fig. 8a, b) deviated at a lower frequency, which demonstrates an altering of the electron transfer process, including a diffusion-limiting step [50]. The electrochemical parameters of the fitted equivalent circuit are tabulated in Table 7. The value of R'_p, continuously increases with an increase in the inhibitor concentration of 5c and 7; as a result the inhibition efficiency increased to its maximum value of 93.2% and 98.5%, respectively after 30 minutes of mild steel immersion in 100 ppm, as shown in Table 7. From Table 7, it was also found that the CPE value decreased with an increase in the inhibitor concentration. The lower n values at the higher concentrations of 5c or 7 can be attributed to an increase in the adsorption of the inhibitors on the surface, thereby suggested to increase the heterogeneity of the mild steel coupon surface.

Bode plots for magnitude or phase angle versus frequency in a Randle equivalent circuit are shown in Fig. 8c-f. In Fig. 8c, d the value of R_s can be obtained from the horizontal plateau region at high frequency, which is almost constant and is not affected by an increase in the inhibitor concentration in the solution [51]. However, the R_p can be determined from the Z magnitude at low frequency; this increases with an increase in the concentration of 5c or 7; this consequently increases the polarization resistance. In Fig. 8e, f a Bode plot of the phase angle versus frequency curve shows a peak shape and maximum angle value at intermediate frequency, which increases with an increase in the inhibitor concentration. These results indicate that the thickness of the surface increases as a result of an additional amount of inhibitor adsorbed on the mild steel surface, and therefore decreases the value of the capacitance. The outcomes of Nyquist and Bode plots confirm the findings that were obtained from the Tafel and LPR methods.

3.5. Adsorption isotherms

The inhibitor molecules employed to study the surface coverage (θ), are presented in Tables 1-7. The inhibition efficiencies (η) is equal to the surface coverage (θ) at lower concentrations where the mild steel coupon surface forms a monolayer coverage. However, at higher concentrations the surface coverage changes from monolayer to multlilayer, and no longer maintains the linear relationship. The gravimetric method in 1 M HCl (Table 1), and 0.5 M H_2SO_4 (Table 2), and Tafel extrapolations in 1 M HCl (Table 5) and CO_2-saturated 0.5 M NaCl (Table 6) were used to determine the θ. The θ and C (the concentration in ppm was translated into mol L^{-1}) were used to find the best among the more frequently used adsorption isotherms described elsewhere in the literature [45].

The correlation coefficient was determined using a Temkin, Langmuir, Frumkin and Freundluich isotherm, which indicated that the inhibitor molecules in 1 M HCl [Fig. 9 (a)], as well as 0.5 M H_2SO_4 [Fig. 9 (b)], fitted the best for the Temkin adsorption isotherm, and CO_2-saturated 0.5 M NaCl [Fig. 9 (c)] fitted the best for the Langmuir adsorption isotherm (Table 8). However, some of the inhibitors demonstrated good fit for both the Temkin and the Langmuir adsorption isotherms.

Eq. (6) relates the K_{ads} to the free energy of adsorption (ΔG^o_{ads}):

$$K_{ads} = \frac{1}{55.5} \exp\left(\frac{-\Delta G^{\circ}_{ads}}{RT}\right) \quad (6)$$

The values of K_{ads} and ΔG^{o}_{ads} are summarized in Table 8. The negative values of ΔG^{o}_{ads} (Table 8) ensure the spontaneity of the adsorption process.

Generally, the values of ΔG^{o}_{ads} up to –20 kJ mol^{-1} can be attributed to physisorption, while those ranging between –80 to –400 kJ mol^{-1} can be recognized as chemisorption.

The calculated $-\Delta G^{o}_{ads}$ values in the range 48 - 77 kJ mol^{-1} in 1 M HCl, 45- 54 kJ mol^{-1} in 0.5 M H_2SO_4 and 32 - 42 kJ mol^{-1} in CO_2-saturated 0.5 M NaCl indicate that the π and non-bonded electrons induce the inhibitor molecules in various media to undergo a combination of both electrostatic adsorption and chemisorption in the anodic sites *via* overlapping with the low-lying vacant d-orbitals of iron [51,52].

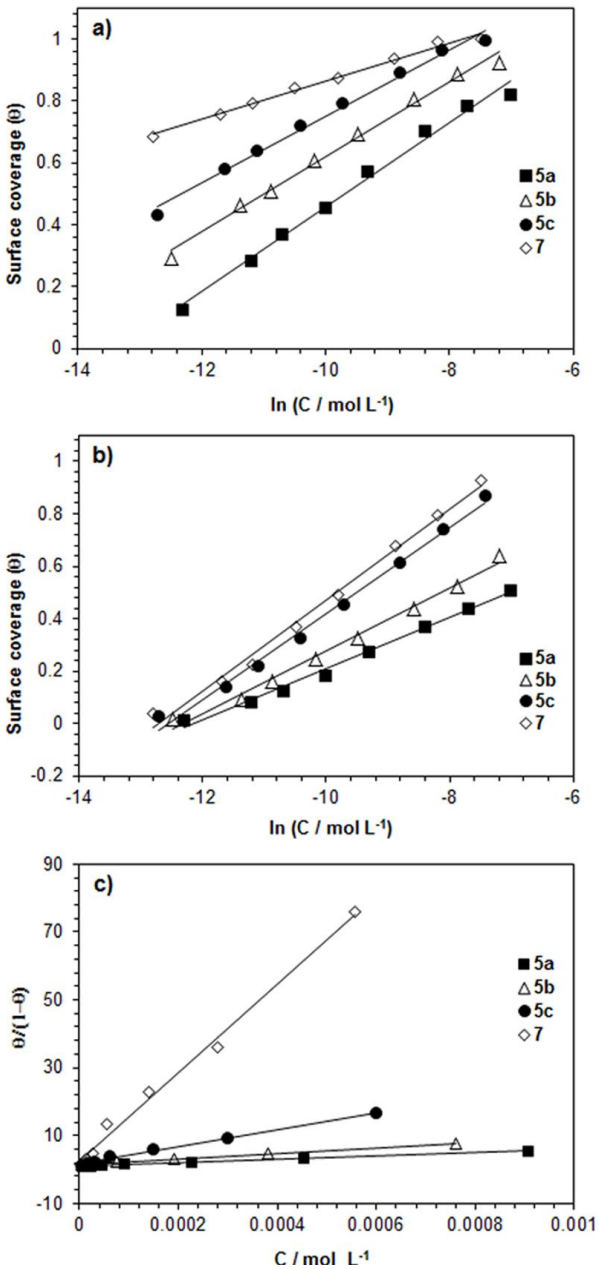

Figure 9. (a) Temkin adsorption isotherm of **5** and **7** in 1 M HCl at 60 ºC, (b) Temkin adsorption isotherm of **5** and **7** in 0.5 M H_2SO_4 at 60 ºC and (c) Langmuir adsorption isotherm of **5** and **7** in CO_2-saturated 0.5 M NaCl at 40 ºC.

Table 8. Thermodynamic parameters of the mild steel dissolution in the presence of **5a-c** and **7**.

Compound	Isotherm used	Correlation coefficients (R^2)	K_{ads} (L mol^{-1})	ΔG^o_{ads} (kJ mol^{-1})
		in 1.0 M HCl (60 ºC) (Gravimetry)		
5a	Temkin	0.9912	6.27 E+5	−48.1
5b	Temkin	0.9923	3.63 E+6	−52.9
5c	Temkin	0.9902	2.29 E+7	−58.0
7	Temkin	0.9908	2.63 E+10	−77.5
		in 0.5 M H_2SO_4 (60 ºC) (Gravimetry)		
5a	Temkin	0.9913	5.79 E+6	−54.2
5b	Temkin	0.9911	2.23 E+5	−45.2
5c	Temkin	0.9918	2.85 E+5	−45.9
7	Temkin	0.9922	3.29 E+5	−45.3
		in 0.5 M NaCl/CO_2 (40 ºC) (Tafel)		
5a	Langmuir	0.9947	5.10 E+3	−32.7
5b	Langmuir	0.9931	8.07 E+3	−33.9
5c	Langmuir	0.9936	2.51 E+4	−36.6
7	Langmuir	0.9926	1.31 E+5	−41.1
7[a]	Langmuir	0.9949	1.97 E+5	−42.2

[a] via LPR

3.6. Surface tension

The surface tension γ and CMC of the inhibitor samples 5c and 7 are measured in CO_2-saturated 0.5 M NaCl at 40 ºC, and the results are presented in Table 9.

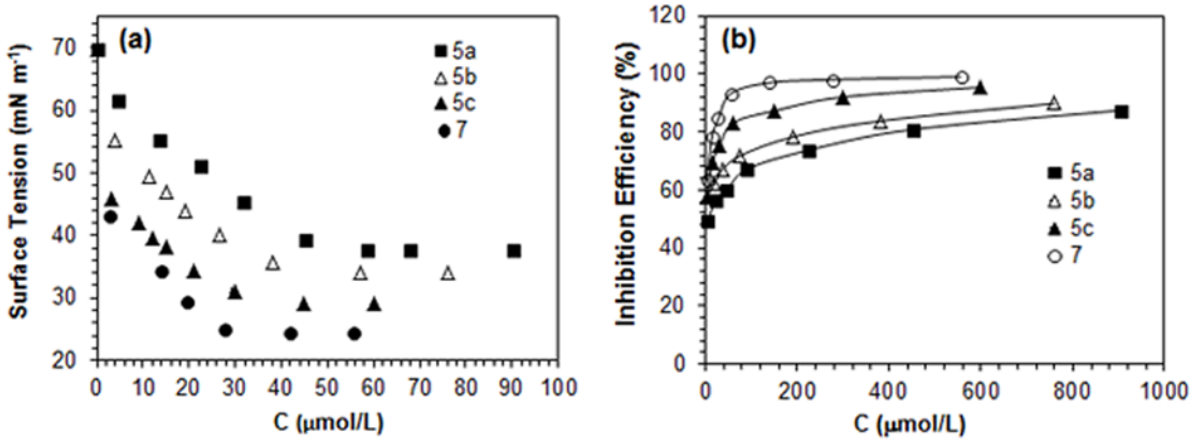

Figure 10. (a) Surface tension versus concentration, and (b) Inhibition efficiency versus concentrations profile of **5** and **7** in CO_2-saturated 0.5 M NaCl solution at 40 ºC.

Fig. 10a shows the plot of surface tension γ against the concentration of the inhibitors, while Fig. 10b shows the η% versus concentration profiles. In this work, the inhibitor molecules 5 and 7 were determined in order to shed light on the adsorption process: Do these inhibitor molecules prefer micellization prior to adsorption or vice versa? As expected, the CMC, as well as the surface tension at the CMC, was found to be progressively lower with the hydrophobic groups such as those with an aliphatic bicyclic structure and/or an increased length of alkyl chain [40]. For inhibitor molecule 7 at a concentration of 10 ppm, the θ of 87% confirmed that the inhibitor molecule covered most of the surface before its concentration reached the CMC value of 9.42 ppm (i.e. 26.2 μM) in CO_2-saturated 0.5 M NaCl (Fig. 10, Table 9).

Table 9. Surface properties of inhibitor compounds **5a-c** and **7** in CO_2-saturated 0.5 M NaCl at 40 ºC

Compound	Surface tension (mN m^{-1})	C_{cmc} (μmol L^{-1})	C_{cmc} (ppm)	$\Delta G°_{mic}$ (kJ mol^{-1})
5a	38.4	45.6	10.1	-26.0
5b	34.4	36.7	9.66	-26.6
5c	30.0	28.5	9.50	-27.2
7	25.2	26.2	9.42	-27.5

A closer look at the CMC values (Fig. 10a, Table 9) and the surface coverage data (Fig. 10b, Table 6) reveals that the inhibitor molecules cover most of the mild steel coupon surface by the formation of a monolayer film before reaching their CMC, after which a multilayer can form due to the adsorption of micelles that can provide further protection up to a certain extent [53]. The ΔG^o_{ads} values (≈ – 42 kJ mol^{-1}, Table 8) are more negative, compared with the corresponding ΔG^o_{mic} (≈ – 27 kJ mol^{-1}, Table 9), which further indicate that the adsorption of inhibitor molecules on the mild steel coupon surface is preferred over micellization.

4. CONCLUSIONS

A series of new isoxazolidine derivatives of aldehyde motifs were synthesized using a widely used nitrone cycloaddition reaction. The synthesized compounds, particularly compound 7, was found to be an excellent corrosion inhibitor in HCl, H_2SO_4 and CO_2-saturated saline media. At a concentration of 20 ppm, inhibitor molecules 5a, 5b, 5c and 7 imparted inhibition efficiencies of 57.1, 69.1, 95.2 and 99.1% in 1 M HCl at 60 ºC (Table 1), and 67.2, 71.9, 83.2 and 97.4%, respectively in CO_2-saturated 0.5 M NaCl at 40 ºC (Table 3). The synthesized inhibitor molecules were employed to determine the inhibition efficiencies in CO_2-saturated 0.5 M NaCl at high pressure (9.9 atm) and high temperature (120 ºC). At a concentration of 200 ppm, the inhibitor molecules 5a, 5b, 5c, 7, and commercial inhibitors QI 80 and ARMOHIB 219 demonstrated η % of 57.7, 68.9, 79.2, 86.3, 81.0 and 82.7, respectively. The inhibitor compound 7 performed better than 5a-c and the two commercial inhibitor samples. The greater reduction of i_{corr} values in the anodic branch of Tafel plots and the shift of the E_{corr} values in the anodic direction established that the inhibitor molecules acted mainly as

anodic inhibitors. The ΔG^{o}_{ads} points towards both physisorption, as well as chemisorption, of the inhibitors on the metal surface. The presence of an electron-rich aromatic ring, along with a hydrophobic chain and the bicyclic structure in the inhibitors, may help to lock them strongly on the metallic surface. The adsorption of inhibitor molecules in HCl and H_2SO_4 follows the Temkin adsorption isotherm model. However, CO_2-saturated 0.5 M NaCl follows the Langmuir adsorption isotherm model. The inhibitor molecules act as a surface active molecule as they lower the surface tension; the surface coverage data and CMC values demonstrated that the inhibitor molecules prefer to undergo adsorption on to the metal surface rather than micellization. A better surface coverage provided by the compound *p*-9-[hexahydropyrrolo(1,2-b)isoxazol-2-yl]nonyloxybenzaldehyde 7 is a significant finding that would indeed be helpful in designing better isoxazolidine corrosion inhibitors having an aliphatic bicyclic ring with a hydrophobic chain longer than the current nonyloxy group.

ACKNOWLEDGEMENTS
The use of research facilities provided by King Fahd University of Petroleum & Minerals and the financial assistance of the Deanship of Scientific Research, KFUPM (Startup grant: IN121036) are gratefully acknowledged.

References

1. C. Volkan, *Corrosion Chemistry*, John Wiley & Sons, New Jersey (2011).
2. P. C. Vasant, G. K. Bansal, *Int. J. Chem. Sci. Appl.*, 4(1) (2013) 1.
3. I. M. Gadala, A. Alfantazi, *Corros. Sci.*, 82 (2014) 45.
4. E. Kusmierek, E. Chrzescijanska, *Mater. Corros.*, 66(2) (2015) 169.
5. V. S. Sastri, *Corrosion Inhibitors, Principles and Application*, John Wiley & Sons, New Jersey (2001).
6. F. Bentiss, F. Lagrenee, M. Traisnel, *Corrosion*, 56 (2000) 733.
7. A. O. James, N. Oforka, K. A. Olusegun, *Int. J. Electrochem. Sci.*, 2 (2007) 278.
8. S. A. Odoemelam, N. O. Eddy, *Surf. Sci. Technol.*, 24 (2008) 65.
9. O. Benali, L. Larabi, Y. Harek, *J. Appl. Electrochem.*, 39 (2009) 769.
10. X. H. Li, S. D. Deng, F. Fu, G. N. Mu, *J. Appl. Electrochem.*, 39 (2009) 1125.
11. R. Singh, *Pipeline Integrity Handbook: Risk Management and Evaluation*, Gulf Professional Publishing, Waltham, MA (2014).
12. H. A. Craddock, S. Caird, H. Wilkinson, M. Guzmann, *SPE Projects, Facilities & Construction*, 2(4) (2007) 1.
13. R.W. Revie, H. H. Uhlig, *Corrosion and Corrosion Control*, John Wiley & Sons, New Jersey (2008).
14. M. Elachouri, S. Kertit, H. M. Gouttaya, B. Nciri, Y. Bensouda, L. Perez, M. R. Infante, K. ElKacemi, *Prog. Org. Coat.*, 43 (2001) 267.
15. M. Finšgar, J. Jackson, *Corros. Sci.*, 86 (2014) 17.
16. M. Abdallah, *Corros. Sci.*, 44 (2002) 717.
17. J. Zhang, X. L. Gong, W. W. Song, B. Jiang, M. Du, *Mater. Corros.*, 63 (2012) 636.
18. R. A. Prabhu, T. V. Venkatesha, A. V. Shanbhag, G. M. Kulkarni, R. G. Kalkhambkar, *Corros. Sci.*, 50 (2008) 3356.
19. N. Caliskan, E. Akbas, *Mater. Corros.*, 63 (2012) 231.
20. K. Yesim, G. Seda, E. Asli, *Prot. Met. Phys. Chem. Surf.*, 48 (2012) 710.
21. V. Jovancicevic, S. Ramachandran, P. Prince, *Corrosion*, 55 (1999) 449.

22. S. Ramachandran, B. L. Tsai, M. Blanco, H. Chen, Y. Tang, W. A. Goddard III, *Langmuir*, 12 (1996) 6419.
23. A. M. Abdel-Gaber, M. S. Masoud, E. A. Khalil, E. E. Shehata, *Corros. Sci.*, 51 (2009) 3021.
24. X. Li, S. Deng, H. Fu, *Corros. Sci.*, 62 (2012) 163.
25. L. Wang, S. W. Zhang, Q. Guo, H. Zheng, D. M. Lu, L. Peng, J. Xion, *Mater. Corros.* 66(6) (2015) 594.
26. D. Daoud, T. Douadi, S. Issaadi, S. Chafaa, *Corros. Sci.*, 79 (2014) 50.
27. A. Edwards, C. Osborne, S. Webster, D. Klenerman, M. Joseph, P. Ostovar, M. Doyle, *Corros. Sci.*, 36 (1994) 315.
28. G. McIntire, J. Lippert, J. Yudelson, *Corrosion*, 46 (1990) 91.
29. A. Yildirm, M. Cetin, *Corros. Sci.*, 50 (2008) 155.
30. S. A. Ali, H. A. Al-Muallem, S. U. Rahman, M. T. Saeed, *Corros. Sci.*, 50 (2008) 3070.
31. S. Rengamani, S. Muralidharan, M. A. Kulandainathan, S. V. Iyer, *J. Appl. Electrochem.*, 24 (1994) 355.
32. S. A. Ali, A. M. El-Shareef, R. F. Al-Ghamdi, M. T. Saeed, *Corros. Sci.*, 47 (2005) 2659.
33. M. Finsgar, J. Jackson, *Corros. Sci.*, 86 (2014) 17.
34. S. A. Ali, H. A. Al-Muallem, M. T. Saeed, S. U. Rahman, *Corros. Sci.*, 50 (2008) 664.
35. S. A. Abd El–Maksoud, *Int. J. Electrochem. Sci.*, 3 (2008) 528.
36. Ali, S. A.; Saeed, M. T.; Rahman, S. U. *Corros. Sci.*, 45 (2003) 253.
37. S. A. Ali, A. J. Hamdan , A. A. Al-Taq, S. M. J. Zaidi, M. T. Saeed, *Corros. Eng. Sci. Techn.*, 46 (2011) 796.
38. M. A. J. Mazumder, H. A. Al-Muallem, M. Faiz, S. A. Ali, *Corros. Sci.*, 87 (2014) 187.
39. H. J. Butt, K. Graf, M. Kappl, *Physics and Chemistry of Interfaces*, Wiley-VCH, Weinheim (2003).
40. K. Videm, A. Dugstad, *Mater. Performance*, 28 (1989) 63.
41. M. A. J. Mazumder, H. A. Al-Muallem, S. A. Ali, *Corros. Sci.*, 90 (2015) 54.
42. A. Padwa, W. H. Pearson, *Synthetic application of 1,3-dipolar Cycloaddition Chemistry toward Heterocycles and Natural products*, John Wiley & Sons, New Jersey (2003).
43. B. Chakraborty, A. Samata, C. D. Sharma, N. Khatun, *Ind. J. Chem.*, 53 (2014) 218.
44. S. Z. Duan, Y. L. Tao, *Interface Chemistry*, Higher Education Press, Beijing (1990).
45. P. C. Okafor, X. Liu, Y. G. Zheng, *Corros. Sci.*, 51 (2009) 761.
46. F. Bentiss, M. Triasnel, M. Lagrenee, *Corros. Sci.*, 42 (2000) 127.
47. M. Erbil, *Chim. Acta Turc.*, 1 (1988) 59.
48. M. *Ö*zcan, E. Karadag, I. Dehri, *Colloids Surf. A Physicochem. Eng. Aspects*, 316 (2008) 55.
49. *R. Yildiz, T. Doğan, İ. Dehri, Corros. Sci.*, 85 (2014) 215.
50. X. Chen, Y. Wang, J. Zhou, W. Yan, X. Li, J. J. Zhu, *Anal. Chem.*, 80 (2008) 2133.
51. I. L. Rozenfeld, *Corrosion Inhibitors*, MacGraw-Hill, New York (1981).
52. L. Afia, R. Salghi, L. Bammou, E. Bazzi, B. Hammouti, L. Bazzi, A. Bouyanzer, *J. Saudi Chem. Soc.*, 18(1) (2014) 19.
53. K. Esumi, M. Ueno, *Structure Performance Relationships in Surfactants*, Marcel Dekker Press, New York (2003).